Characterization of the stationary states of a dilute vibrofluidized granular bed

P. Sunthar and V. Kumaran

Department of Chemical Engineering, Indian Institute of Science, Bangalore 560 012, India

(Received 16 April 2001; published 21 September 2001)

This paper reports two phenomena in an event driven simulation of a dilute vibrofluidized granular material in two dimensions. Both phenomena show inhomogeneity in the horizontal direction. They are convection rolls similar to the Rayleigh-Bénard thermal convection in fluids, and a clustering instability, where the bed spontaneously phase separates into coexisting dense and dilute regions. Detailed investigations show that these are different from the known instabilities in a vibrated granular medium. Characterization of these instabilities is carried out with a phase diagram using suitable parameters from the kinetic theory of vibrofluidized beds.

PACS number(s): 45.70.Qj, 47.20.Bp

I. INTRODUCTION

Granular materials subjected to vertical vibrations often show complex behavior, such as convection rolls, waves, and clustering. One of the earliest studies on convection rolls is by Faraday [1], who observed these patterns in a powder driven by a loudspeaker membrane. In general, convection rolls have been observed in situations where the amplitude of oscillation is small and the densities are very close to the density of close packing [2–5]. Ramírez *et al.* [6] have reported convection rolls in granular systems ''heated'' from below and in the presence of gravity. The system is confined by a top wall and the density in the vertical direction is nearly constant. The instability seems to be the granular analog of the classical Rayleigh-Bénard instability of a heated liquid [7]. When the amplitude of bottom wall vibrations is comparable to the bed height, the top surface becomes unstable and forms a periodic wavy pattern with peaks and troughs [8–10].

Eggers [11] simulated a vibrated bed under gravity with two compartments separated by a wall that allows particles from one side to the other through a small slit at a given height. For vigorous shaking the populations in the two halves remain equal, but at a lesser rate of shaking the density of particles on one side is different from that on the other. It is also shown that such a stationary state can be captured by a flux balance of particles from one side to the other calculated by simple kinetic theory [12]. The occurrence of large scale inhomogeneities in industrial vibrated beds is reported in [13]; these seem to be similar in nature to a two-phase coexistence, but the instability disappears when the surrounding air medium is evacuated. A two-dimensional layer of particles on a vibrating surface exhibits different states depending on the density and the ratio Γ of the acceleration amplitude of the vibrating surface and the acceleration due to gravity [14].

In general, the onset of instabilities in vibrated granular media depends on many parameters, such as the dynamics of the bottom wall, amplitude of bottom wall oscillations [15], sidewall interaction [2,3], and inherent inelastic nature of particle collisions (such as viscoelastic, friction, etc.) [4]. Previous studies [16,17] have used the ratio of accelerations Γ, the frequency of vibrations, and the coefficient of restitution e as parameters to characterize the formation of patterns.

Savage [15] also described the velocity of circulatory patterns in a vibrated bed in terms of the amplitude and frequency of vibrations, and considered the energy transfer mechanism to be due to the propagation of acoustic waves in the medium. It has also been shown that Γ alone cannot specify the degree of fluidization independently of the system parameters [18]. Detailed studies have shown that the velocity distribution functions can be very different from the Gaussian distribution [19–22]. This makes it difficult to understand the mechanism and the onset of instabilities in a vibrated granular medium. The goal of the present work is to start with a simple system (which can be correctly parametrized using the nondimensional parameters of the kinetic theory of vibrated granular materials [12]) and to explore the parameter space around this state for possible instabilities. The phenomena found are a convection roll instability and a phase separation or clustering instability, which are, in some ways, similar to those found in [6] and [11], respectively. One of the striking features of these instabilities is that a change in one of the parameters causes a transition between these two apparently very different states.

The instabilities reported in the present study differ from previous ones in two major respects.

(1) These are observed in a low density regime, where the area fraction of the particles is small, i.e., the mean free path is large compared to the particle diameter. This is in contrast to previous studies [5,14] where the mean free path is less than the particle diameter. Therefore, it is observed that the steady state before the onset of large scale motion can be accurately described by kinetic theory techniques.

(2) In the present case, the frequency of the base vibration is large compared to the frequency of oscillation of the bed, and the amplitude is small compared to the mean free path of the particles. Consequently, the amplitude and frequency of the base are not relevant parameters in determining the state of the bed and the only relevant parameter is the energy transfer from the base to the particles in discrete particle collisions. In order to show this, we considered two types of simulation; the first is a real vibrating base and the second is a base that is fixed at a location but provides random energy similar to a vibrating base. The two simulations give similar results, indicating that the base amplitude and frequency are not important parameters in this regime. This is in contrast to the systems considered in, for example, [8–10,15], where the

periodicity of the vibrations is coupled to the dynamics.

Other qualitative differences between the present instabilities and those reported earlier are discussed in detail later.

Since we are interested in the dilute limit, it is useful to characterize the system by the parameters relevant for a dilute vibrofluidized bed in the limit where the area fraction is small and the coefficient of restitution is close to 1 [12]. This system can be characterized by four parameters, viz., $N\sigma$, ϵ, ν^0, and ϵ_f [23]. However, the relevant parameters are $N\sigma$, which gives the number of monolayers of particles at rest, and the parameter $\epsilon \equiv (U_0^2/T)$, which is a measure of the ratio of the dissipation in a collision to the average energy of a particle. Here N is the number of particles per unit width, σ is the particle diameter, U_0^2 is the mean square velocity of the vibrating surface, and T is the mean square velocity of the particles. It was shown that in the limit $(1-e^2) \ll 1$, the parameter ϵ is given by [12]

$$\epsilon = \frac{U_0^2}{T} = \frac{\pi N \sigma (1-e^2)}{2\sqrt{2}}. \tag{1}$$

The area fraction of particles ν in the dilute limit is exponentially decaying in the vertical direction, and is given by

$$\nu = \nu^0 e^{-gz/T} \tag{2}$$

where $\nu^0 = \pi N g \sigma^2/(4T)$ is the area fraction of particles at the bottom of the bed and g is the acceleration due to gravity. The parameter $N\sigma$ is varied in the range 0.5–30 and ϵ is varied in the range 0.05–3. The area fraction at the bottom is kept at a constant value $\nu^0 = 0.077$.

The other parameters usually used for characterizing pattern formation in vibrated granular systems are not relevant for the present study.

(1) The ratio of the frequency of oscillation of the bed under gravity $(g/\sqrt{T})$ and the frequency of the bottom wall oscillations (ω_w) is represented by the small parameter $\epsilon_f \equiv g/2\pi\sqrt{T}\omega_w$, which is maintained at a constant value of 0.01 in the simulations, so that there are no correlated collisions of the bed with the bottom wall.

(2) If the layer is considered as a block, the ratio of accelerations is $\Gamma \equiv U_0 \omega_w/g$. In terms of the present notation $\Gamma \sim \sqrt{\epsilon}/\epsilon_f$, and varies in the range 10^2–10^4.

(3) The ratio of the amplitude a_w of the bottom wall vibrations to the mean free path, which is $\sim \epsilon_f N\sigma \sqrt{\epsilon}$, varies in the range (5×10^{-4})–0.04, so that the wall does not induce any mean motion in the bed.

In the present study, we consider the effects of varying $N\sigma$ and ϵ; the other parameters are kept constant at the values mentioned above. In this parameter regime, the dynamics of the bed is coupled to that of the bottom wall only through the energy transfer to the particles (by random collisions with the wall), and the mean motion of the bed is not correlated to the dynamics of the bottom wall. Therefore, the periodicity of the bottom wall vibration does not induce a periodic motion in the flow. This is confirmed by the observation that the instabilities are observed even when the bottom wall is given a random velocity whose probability distribution is identical to that of the vibrated wall.

II. SIMULATION PROCEDURE

A hard sphere molecular dynamics simulation, also known as event driven simulation, is best suited to studying rapid granular flows [24]. An efficient way to incorporate a large number of particles in an event driven simulation is the delayed state update algorithm (DSA) [25]. We have employed the DSA to simulate a large system of granular materials with particles $\mathcal{O}(10^4)$.

The simulation cell is a box containing N circular disks per unit width. The gravitational acceleration force g acts vertically downward. There are two sidewalls and the top is left open. Interparticle collisions are inelastic, and are characterized by a constant coefficient of restitution e. For the sake of simplicity, the interactions of the particles with all three walls are assumed to be elastic. The other parameters are varied according to the prescription given in the previous section. Additionally, for most of the simulations, the width of the simulation cell is maintained at a constant value of 1400, unless otherwise stated. The physical parameters for the base state $\epsilon = 0.1$, $N\sigma = 10$, $\nu^0 = 0.077$, and $\epsilon_f = 0.01$ are as follows:

$$e = 0.995\,488, \quad N = 10, \quad \sigma = 1,$$

$$g = 0.098\,039\,4, \quad U_0 = 1,$$

$$\text{with} \quad a_w = 0.051\,335\,7, \quad \omega_w = 19.479\,6.$$

In the following presentation, the length and time units are obtained from σ and σ/U_0 respectively, except in the experimental values suggested in Sec. V.

After the system attains a steady state, the system is probed for inhomogeneities by the following methods.

(1) The system is divided into 100 cells in the horizontal direction and 20 in the vertical direction up to a height equal to $2T_0/g$. This corresponds to about N particles per cell near the bottom wall in a cell of dimension 10×14. The local time averaged velocity of the particles in each cell is calculated. Convection rolls can be observed by plotting the streamlines of the local velocity.

(2) Visual inspection for clustering and monitoring a tracer particle in a graphics animation tool are performed.

(3) Fluctuations in the number density of particles per unit length in the horizontal direction are monitored. The bed is divided in the horizontal direction into several bins. The local number of particles per unit width N_x in a bin is measured. Since the density per unit width for the entire bed is N, the scaled density fluctuation can be defined as

$$\tilde{N}_x = \frac{N_x}{N} - 1. \tag{3}$$

A plot of the variation in $\tilde{N}_x$ across the bed in time shows the evolution of the bed from the homogeneous state to an inhomogeneous one.
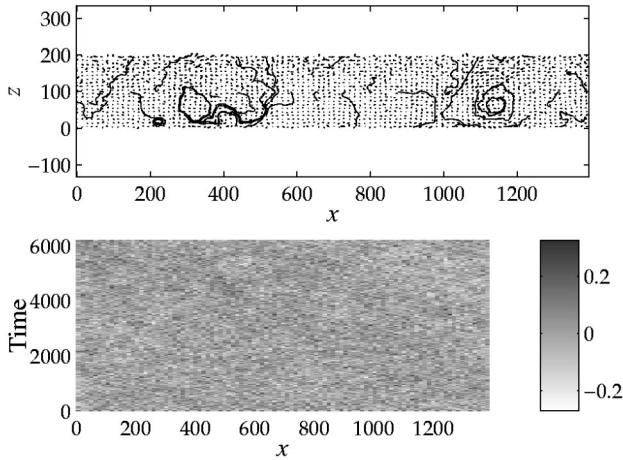
FIG. 1. Plots showing the states of the bed for a homogeneous case. The first plot shows the local velocity vectors and the second plot shows the variation of the scaled density fluctuation $\tilde{N}_x$ with time and the horizontal direction x. There are no convection and no density variation in the horizontal direction. The parameters used for this simulation are $N\sigma = 10$, $\epsilon = 0.3$, and $\nu^0 = 0.077$.

III. CONVECTION ROLLS

For low values of ϵ and $N\sigma$, the temperature of the bed is nearly independent of height, as expected from kinetic theory. The density is exponentially decaying in the vertical direction and homogeneous in the horizontal direction. The homogeneous state is shown in Fig. 1.

As ϵ is increased, the dissipation increases and the system develops a temperature gradient that is adverse to the density stratification. The homogeneous state becomes unstable and the bed develops convection rolls as seen in Fig. 2. These rolls are qualitatively similar to the Rayleigh-Bénard convection rolls of heated films of liquid [7]. There is no preferred direction of motion along the sidewalls, since they are elastic. In this example, both upward and downward motion occur at different time intervals; the location of the convection roll is unsteady in time. The height of the convection roll is of the order of the vertical length scale of density variation, which is T_0/g. We now present some more results on the nature of the convection rolls and their dependence on different parameters.

a. Frequency of convection rolls. The frequency of circulation of the convection rolls can be measured by monitoring the coordinates of a tracer particle and determining the Fourier transform of the time variation of its position. To do this, a time series of the coordinates of any one of the particles is determined after the system begins to show convection rolls. It is observed that there is a dominant frequency, and in the case of the system with parameters as in Fig. 2, the ratio of the frequency of circulation to the bottom wall frequency is about 8×10^{-4}. This clearly shows that the dynamics of convection occurs in a much longer time scale compared to the time period of the bottom wall vibration.

b. Effect of ϵ. A low value of ϵ implies a small gradient in temperature, whereas a high value of ϵ implies large temperature and density gradients, where the bed is expected to
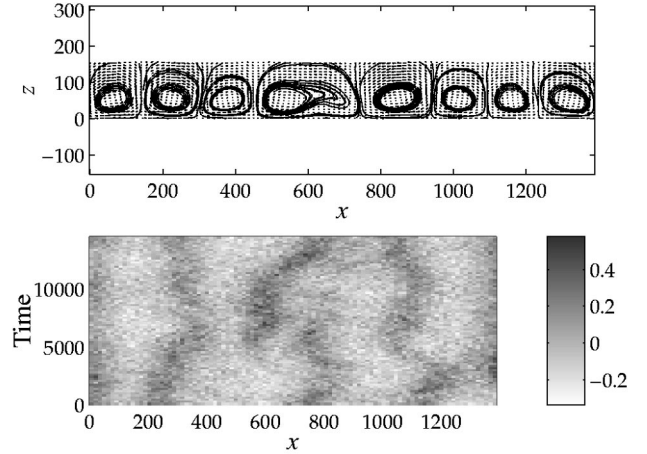

FIG. 2. Convection rolls: Several convection rolls are seen to form along the horizontal direction in the top plot. The plot shows the velocity vectors as well as the streamlines. The height of the roll is nearly equal to the length scale of density variation along the vertical direction. There is no confinement on the top. The bottom plot shows a surface plot of the time evolution of the scaled density fluctuation $\tilde{N}_x$ from a homogeneous initial condition to a variation of density in the horizontal direction. In this case both upward and downward motion occur along the walls during different periods of time, as seen from the alternating light and dark regions near the wall. The parameters used for this simulation are $N\sigma = 10$, $\epsilon = 0.75$, and $\nu^0 = 0.077$.

be unstable due to buoyancy effects. Therefore, at constant $N\sigma$, an increase in ϵ induces a transition from a homogeneous state (Fig. 1) to an inhomogeneous state (Fig. 2). Within the inhomogeneous state, an increase in ϵ increases the amplitude of the local density fluctuations and decreases the length scale over which they occur. This can be seen by comparing the values of the maximum scaled density fluctuation which increase from $|\tilde{N}_{max}| = 0.6$ to about 0.75 when ϵ is increased from 0.75 in Fig. 2 to 1.5 in Fig. 3. In Fig. 2 ($\epsilon = 0.75$), there are about five high density bands (implying eight convection rolls) whereas in Fig. 3, with $\epsilon = 1.5$, the number of convection rolls increases to 12.

In [26] it is argued that in the case of a homogeneously cooling state (HCS) the length scale of clustering due to inelastic collisions is given by

$$k^* \sim \frac{\sqrt{(1-e^2)}}{\lambda}, \tag{4}$$

where k^* is the characteristic wave number and λ is the mean free path. The length scale of variation can be determined from the Fourier transform of the scaled density fluctuations in the horizontal direction. In Fig. 4 we see that the characteristic wave number k^* shows a dependence similar to that found in [26] for the HCS. For very large values of ϵ, the bed does not select a particular length scale, as shown in the plots in Fig. 5.
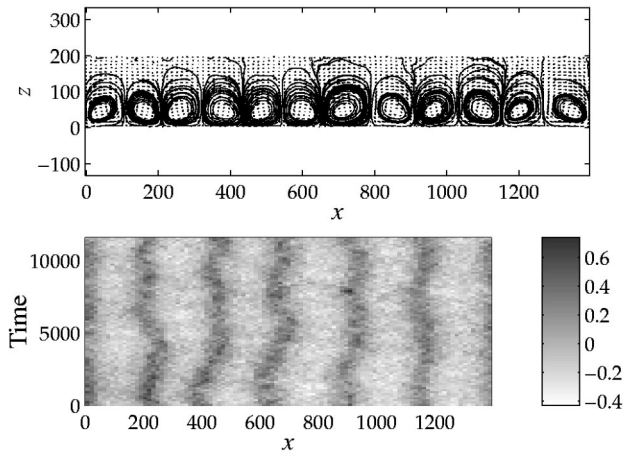
FIG. 3. Effect of increasing ϵ on convection rolls: In general this increases the number of dense bands for a given width and a higher density fluctuation. The parameters used for this simulation are $N\sigma = 10$, $\epsilon = 1.5$, and $\nu^0 = 0.077$. Here, $|\tilde{N}|_{max} = 0.75$. Compare with Fig. 2 which is for a lower ϵ.

c. Effect of the width of the cell. The width of the cell in a simulation is given by $W = N_p / N$. In all the simulations considered the width of the cell is fixed at $W = 1400$. A variation in the width of the cell alters the number of convection rolls, but the wavelength remains unaltered. The convection rolls are also found when the sidewalls are replaced by periodic boundary conditions, although in this case the patterns are observed to be unsteady in time.

A. Effect of the bottom wall driving

We consider two different model walls—a constant temperature wall and a fixed wall with a random velocity that
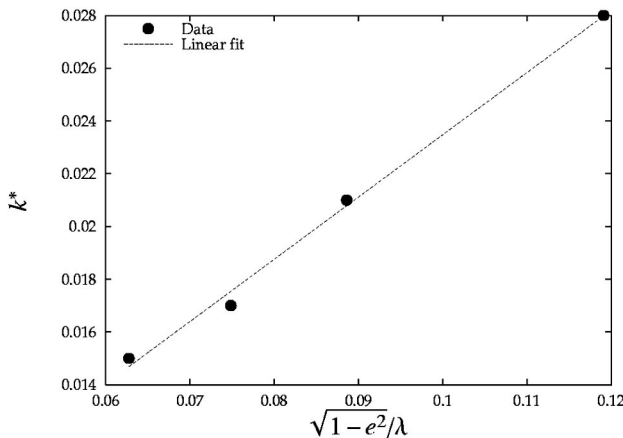
FIG. 4. Variation of length scales of convection in the horizontal direction. The characteristic wavelength (found by Fourier transform of the density fluctuation in the horizontal direction) is plotted against $\sqrt{1-e^2}/\lambda$. To calculate the mean free path the density near the bottom wall is used, which is taken from the simulation data and not from the leading order theoretical results. The slope of the variation here is 0.24. The lengths are nondimensionalized by particle diameter.
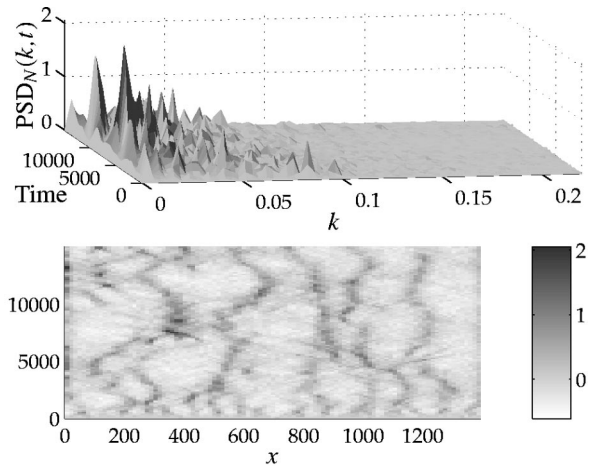

FIG. 5. For very large values of ϵ the system does not seem to select a particular length scale. In this figure the top plot shows the Fourier transform of the density fluctuation in the spatial domain as a normalized power spectrum distribution (PSD) in the wave vector k. The bottom plot shows the evolution of the fluctuation in real space. Both these plots show the nonuniqueness of the length scales of convection. The lengths are scaled by the particle diameter.

has the same distribution as the vibrating surface—and compare the results with those for the vibrating wall with a fixed amplitude.

A constant temperature wall was used in [6] where convection rolls were observed that are similar to the ones we have shown above. The constant temperature wall is simulated by the following algorithm. The collision time of a particle with the wall is calculated by assuming that the wall is static at $z = 0$. Upon collision, the postcollision velocity of the particle in the vertical direction is chosen randomly from a Gaussian distribution function with a variance T_w, thereby being independent of the precollision velocity. The velocity in the horizontal direction remains unchanged.

In the fixed wall with a random velocity [27], the bottom wall is static at $z = 0$ but during a particle collision event it assumes a velocity, taken randomly from a probability distribution identical to that for the vibrating wall and greater than or equal to the velocity of the particle. The characteristic velocity U_s of the distribution is such that on the average the wall provides the same energy input as the vibrated wall. This is different from the constant temperature boundary condition at the bottom surface since the flux of energy depends on the precollision velocity of the particle.

The parameter set chosen for the following set of simulations is the same as that used in the simulations with a vibrated wall shown in Fig. 2, except for the bottom wall conditions. We choose, by trial and error, a value for the temperature T_w and the characteristic velocity U_s such that the time averaged profiles of density and temperature are close to those of the vibrated wall as obtained in Fig. 2. The density, temperature, and energy flux profiles are shown in Fig. 6 for a vibrated wall, a constant temperature wall, and a fixed wall with random velocity. The width of the cell in these simulations is restricted to $W = 150$ required for observing a single roll.
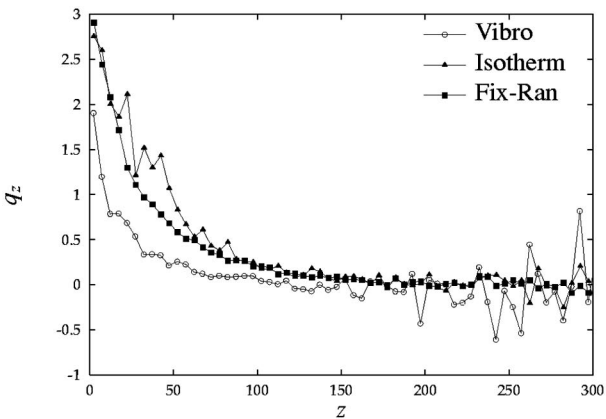
Although the time averaged profiles are nearly identical for the three different systems, we observe in Fig. 7(a) that
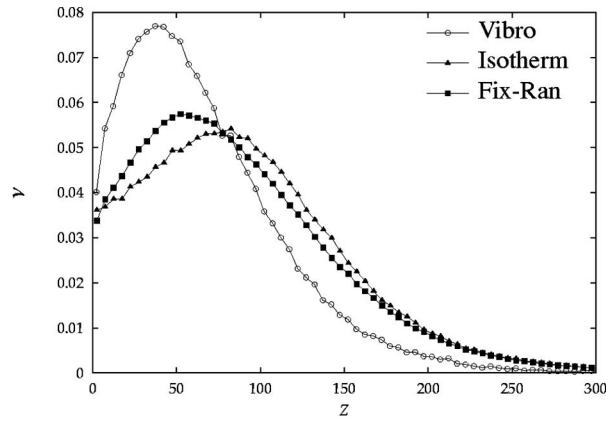
(a) Density
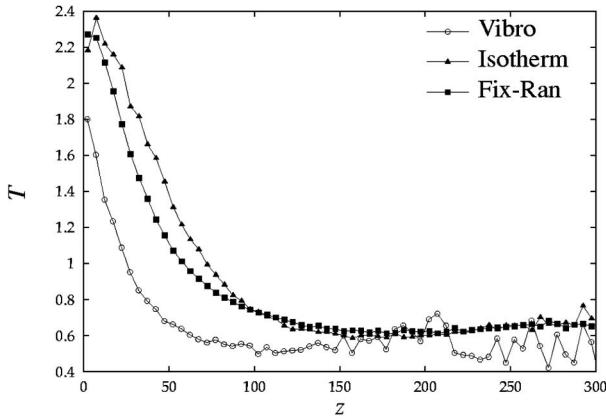
(b) Temperature

(c) Heat flux q_z

FIG. 6. Profiles of variables for different bottom wall drivings—vibrated (Vibro), isothermal (Isotherm), and a fixed wall with random velocity (Fix-Ran). The parameters are chosen so that the profiles closely match those of the vibrated bed. The parameters used for this simulation are $N\sigma = 10$, $\epsilon = 0.75$, and $\nu^0 = 0.077$, corresponding to the vibrated bed. The lengths are scaled by the particle diameter and the energy is scaled by U_0^2.

there is no convection in the constant temperature wall. In contrast, in Fig. 7(b) we see that convection has set in. It is interesting to note that, for both the fixed wall with random velocity and the isothermal wall, the time averaged density and temperature profiles are very close (see Fig. 6), yet the
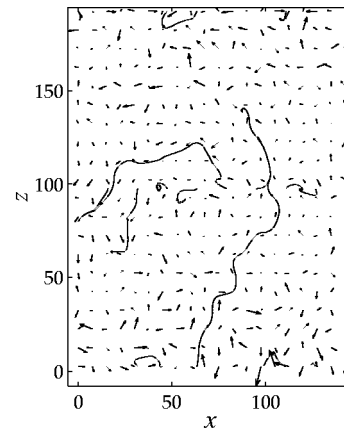
(a) Isothermal wall
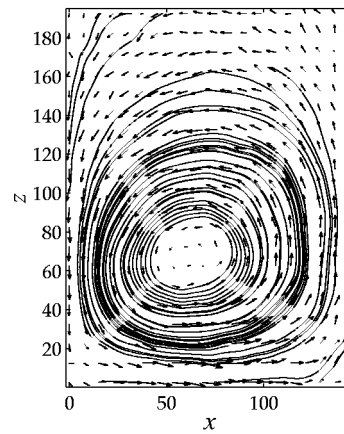
(b) Fixed, random velocity wall

FIG. 7. State of the bed with two different bottom wall drivings. There is no convection in the isothermal wall, whereas the fixed wall with random velocity shows a distinct convection roll.

convection roll and the corresponding horizontal density fluctuation are not observed in the isothermal wall.

A possible explanation for the difference in the behavior of an isothermal and a vibrated wall is as follows. In an isothermal wall, since the postcollision velocity is independent of the precollision velocity, and depends only on the temperature of the wall, the temperature fluctuations in the horizontal direction are damped. In a vibrated wall, the wall vibration only augments the energy of the particles, and does not dampen horizontal fluctuations in the temperature. From the fixed wall simulation, it can also be inferred that the presence of a finite amplitude of the bottom wall vibration is not a necessary condition for the formation of this type of convection roll, so long as the wall only augments the energy of the particles and does not impose a fixed energy. The system with an isothermal wall does develop convection rolls [6], but for values of ϵ larger than that for the fixed wall with random velocity.

B. Discussion

We compare the present results with those of previous studies for convection rolls and demonstrate that the pattern observed here is qualitatively different from the others.

a. Amplitude of bottom wall oscillation. This amplitude plays a major role in the formation of the inhomogeneities in most earlier studies. When the bottom wall amplitude is comparable to the bed height, the bed completely loses contact with the bottom during some phases of the cycle, just like a block of solid being vibrated [28]. For smaller values comparable to the mean free path of the particles the bottom acts as a source of kinetic energy of mean motion inducing compression waves in the medium [15,29]. Also, in [15,30] the bottom wall has a sinusoidal modulation. In the present case, the height of the bed and the mean free path are large compared to the amplitude of the bottom wall. This implies that the wall does not act as a source of compression waves, and the mean motion is developed due to discrete collisions of the particles with the wall. Moreover, the results for the fixed wall (with random velocity) clearly indicate that the amplitude of vibration does not affect the instability.

b. Frequency of bottom wall. In earlier studies on pattern formation in vibrated granular materials, the frequency of bottom wall oscillations is comparable to the frequency of oscillation of the center of mass, that is, the bed undergoes correlated periodic collisions with the bottom wall [9]. In the present simulations, we have ensured that the frequency of particle collisions is small compared to that of the wall vibrations. We also observed that the time period of circulation is much longer than that of the bottom wall, which indicates that the system dynamics is decoupled from the dynamics of the bottom wall.

c. Low densities. Convection rolls have been observed [5] when the amplitude of vibration is small compared to the bed height, but the volume fraction in this case is close to the maximum packing so that the amplitude of vibration is large compared to the mean free path. In contrast, the state of the bed in the present case is like a dilute gas in equilibrium (i.e., an exponentially decaying density profile with convection observed for as low as 0.03 area fraction) and can be characterized by the kinetic theory for dilute gases.

d. Container geometry. The container geometry that we have chosen has two vertical sidewalls and a bottom wall, and the interactions of the particles with the vertical walls are elastic. Convection is observed even when there are no sidewalls, and a periodic boundary condition is used. This is in contrast to earlier studies, where inclined walls [2,3] or an inelastic wall [30] were used. It is known that an inelastic wall leads to a downward movement of particles at the wall because of lower temperature. In the present case, the direction of the convection rolls near the walls is dependent only on the width of the cell, which dictates the total number of convection rolls. Moreover, in the present case, the particles interact with each other by the simple one-parameter (e) inelastic collision model, unlike the viscoelastic particle interaction model in [4].

e. Top wall. The convection rolls reported in [6] are *confined* by a top wall and the density in the vertical direction is nearly constant. We have used a system where the bed is not confined by a top wall, and the density distribution in the vertical direction is exponentially decaying. Stable convection rolls do not seem to have been observed even for gases heated from below, and the closest analog to the present case is the Rayleigh-Bénard convection in a liquid sheet.

f. Nature of driving. In [6] the bottom wall is a constant temperature source, and the energy flux is proportional to the temperature difference at the wall. This dampens horizontal variations in the temperature of the granular material at the wall. We have used a source that mimics a real vibrating wall, and this does not have the same dampening effect on horizontal temperature fluctuations. Although the final state in our system and that in [6] are similar, the nature of driving can alter the transition from a homogeneous to a convection regime.

Additionally, the convection rolls are observed only when the horizontal width of the system is large enough. This could be one reason why this was not observed in the earlier experiments and simulations of finite sized systems. A qualitative understanding of the convective instability can be provided as follows. A spontaneous local fluctuation in the density causes dense regions to flow down and dilute regions to flow up under gravity. The dense regions have a lower temperature than the dilute regions. This temperature fluctuation is further enhanced by the bottom wall driving. The decaying temperature gradient in the vertical direction drives a dense region up by heating it at the bottom. The fluctuation in the density thus grows to form a stable convection roll, where there is a mean motion of particles between the dilute and dense regions.

IV. PHASE SEPARATION

The second kind of instability of the homogeneous state is similar to the clustering instability in granular gases. When the number of layers $N\sigma$ is reduced at constant density, the length scale of variation in the vertical direction decreases. In this case the bed does not show convection; instead, the density fluctuation in the horizontal direction leads to a separation of coexisting regions of high and low densities. This can be seen in the bottom plot of Fig. 8, where a bed that is initially homogeneous starts accumulating particles preferentially on one side, forming a dense cluster. The numerical values of the density fluctuation evolving from a homogeneous state to a two-phase state are shown in Fig. 9. After the formation of two coexisting regions, there is no further variation in the average densities of the two regions, although there is a variation in the position of the interface between the two regions.

A closer view of the particles can be seen in Fig. 10, which is for a still lower $N\sigma$. The transition from the dense to the dilute region is sharper in this case, and there is a continuous exchange of particles from one to the other. The transport of particles from the high density region to the low density region takes place mainly from the top, whereas the reverse transport takes place near the bottom. The formation of the dense region near the left wall in Fig. 9 is a random event; in Fig. 10 the dense region is formed near the right wall. (The initial spatial distribution of particles taken for simulation also matters in this context. It is necessary to ensure that all the rows are filled by particles. Otherwise, it
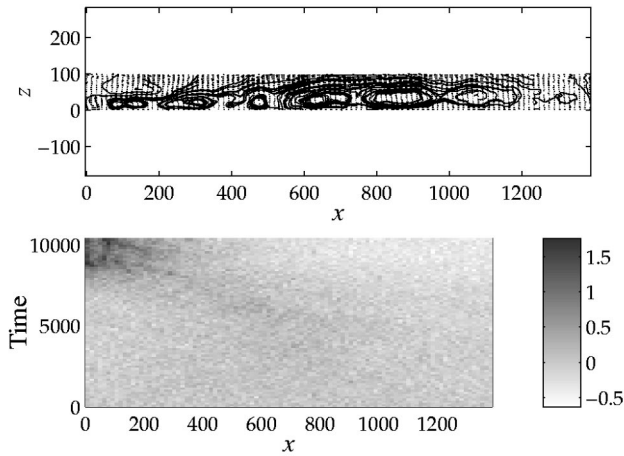
FIG. 8. Clustering of particles near the left wall of the container for a low value of $N\sigma$. The evolution from a homogeneous initial state to a two phase state with the dense on the left and the dilute on the right can be seen in the bottom figure. The average ''width'' of the dense phase remains constant in time from then on. The streamlines in the top figure give an indication of the direction of transfer of particles between the dense and the dilute regions. Here $|\tilde{N}_x|_{max}=1.8$. The parameters used for this simulation are $N\sigma=5$, $\epsilon=0.75$, and $\nu^0=0.077$.

was observed that an initial nonuniformity in the number of layers acts as an imposed density fluctuation.)

The static structure of the two phases can be mathematically represented by the pair distribution function $g(r)$, which is shown in Fig. 11. Here we see that the dilute region is like a gas phase with uncorrelated particle positions and the dense phase is like a liquid phase showing correlations up to a few particle diameters.

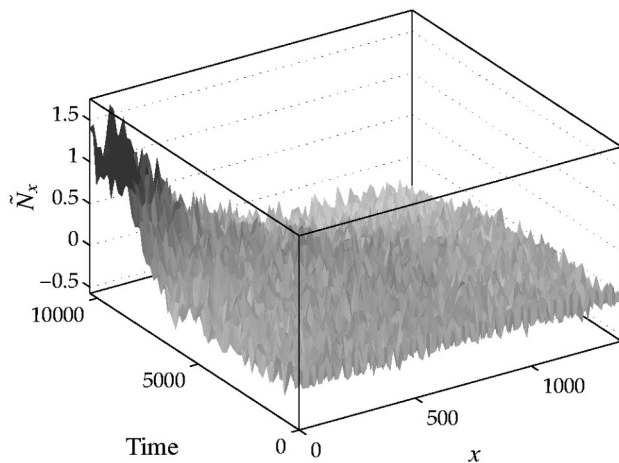Another salient feature of this coexistence is the form of

FIG. 9. A three-dimensional (3D) plot of the evolution of the scaled density fluctuation of Fig. 8. The quantitative evolution in the density can be seen in this figure. The bed has a homogeneous density distribution (averaged around zero) at time $t=0$, which develops a variation along the horizontal direction. The density fluctuation near $x=0$ has a maximum of about 1.5, which sharply decreases to saturate at about -0.4 at $x=1400$.
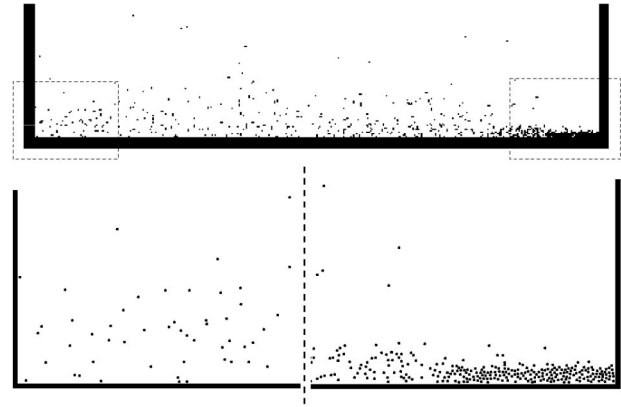

FIG. 10. Exploded view of snapshots of regions near the left and the right walls. A coexistence of the dilute and dense regions can be seen near the right wall. The parameters used for this simulation are $N\sigma=1$, $\epsilon=0.75$, and $\nu^0=0.077$. The transition from the dense to the dilute region is more sharp here than in the previous case. The horizontal width of the cell here is $W=624$.

the horizontal velocity distribution function in the dense phase. Figure 12 shows the velocity distribution functions at two different points—near the left wall and near the right wall of Fig. 10. For each of the plots we have also plotted the Gaussian curve with the same temperature for reference. It is seen that in the dilute region the distribution function is very close to the Gaussian distribution, whereas in the dense region the distribution function shows non-Gaussian tails. Such non-Gaussian distributions have been found in many other granular systems where other kinds of clustering phenomena have been found [19,20,22].

A study of the dependence of the phase separation on different parameters is given below. The effects are similar in nature to those observed in the case of the convection rolls.

a. Effect of ϵ. An increase in ϵ reduces the length scale of formation of dense regions in the horizontal direction. This
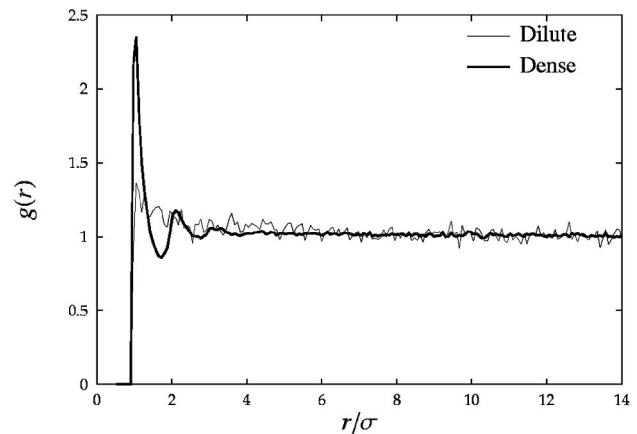

FIG. 11. Pair distribution function in the dilute and dense phases. The static structure of the dilute phase is similar to a gas (with little correlation in position of a pair of particles) and the dense phase is similar to a liquid (with correlation up to few particle diameters).
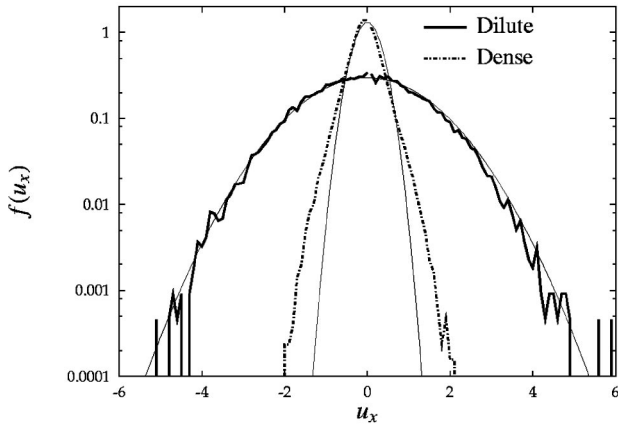
FIG. 12. The distribution functions of horizontal velocities in the dilute and the dense regions are plotted here. A Gaussian curve corresponding to the same local temperature T is also plotted for comparison. It is seen that for the dilute region the distribution function is very close to the Gaussian curve, whereas for the dense region the distribution function shows a non-Gaussian behavior. The velocities are scaled by the bottom wall velocity.

also increases the density of the dense region. The values of the maximum density fluctuation increase from $|\widetilde{N}_{\max}|=1.8$ to about 1.83 when ϵ is increased from 0.75 to 3. For the same width of simulation $W=1400$, when $\epsilon=0.75$ there is one high density region whereas with a higher $\epsilon=3$ the number of dense regions increases to 2.

b. Effect of width of the cell. Changing the width of the cell does not alter the length scale of the density fluctuation or its magnitude. Figure 13 shows the density fluctuation surface for three different widths. The widths of the high and low density regions are nearly the same in the plots. For lower widths, as in Fig. 13(a), there is no phase separation. The formation of the dense regions is also not restricted to the regions near the wall, as shown in Fig. 13(c) where the phase separation occurs at several places and the dense regions coexist with dilute regions on both sides.

c. Effect of the bottom wall driving. If a constant temperature condition is used to drive the bottom wall, phase separation is not observed. This is due to the damping of temperature fluctuations in the horizontal direction by the constant temperature boundary condition at the bottom wall, as observed with the convection rolls.

d. Oscillatory state. The simulations also indicate that the horizontal position of the interface between the high and low density regions fluctuates in time, as shown in Fig. 14. To study the dynamics of the interface, we have plotted the Fourier transform of the density fluctuation. In the second plot of Fig. 14, we see that the dominant peak occurs only in the interface region and is clearly characterized by a single frequency; the corresponding time period (1.6×10^{4}) matches the order of fluctuations seen in the time domain.

Discussion

It was shown in [31] that this state cannot be explained by a simple model for the coexistence of the two phases such as
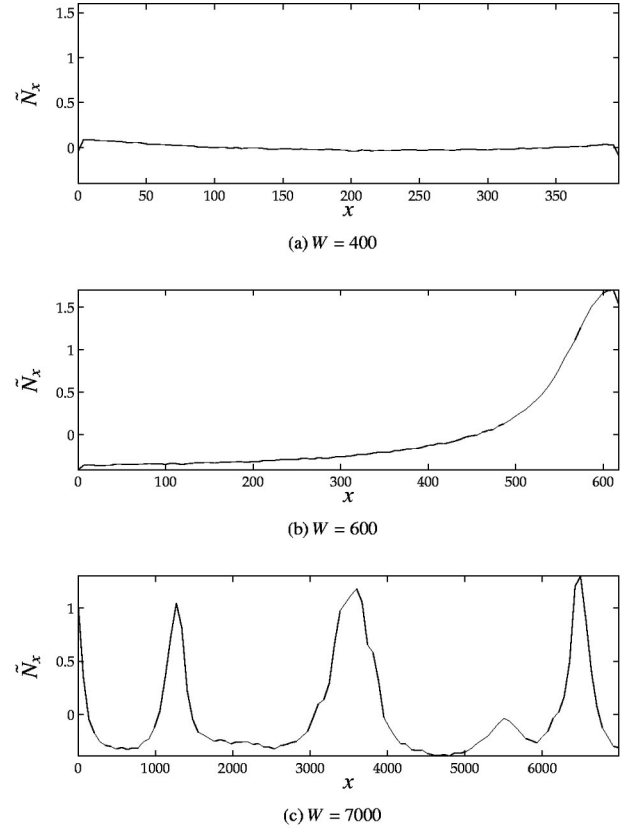

FIG. 13. Effect of width of cell on phase separation. The horizontal variation of the steady state scaled density fluctuation $\widetilde{N}_x$ is shown here for different cell widths. The parameters used for this simulation are $N\sigma=1$, $\epsilon=0.75$, and $\nu^{0}=0.077$. For low widths there is no phase separation, whereas the length scale of separation of the two phases is nearly the same in the other plots. The dense regions coexist with dilute regions on both sides and are not necessarily restricted to near the walls of the container, as seen in (c).

the one reported in [11]. The clustering instability leading to a spontaneous phase separation that we have observed is different from the other types of clustering reported in the literature. Clustering of particles has been reported for a homogeneously cooling system [26,32] where there is no energy input by external driving. In a HCS, the clustering and collapse of particles occur because of dissipation due to inelastic collisions without any energy input. In contrast, the present system is driven by a vibrated wall.

In several reports of "heated" or vibrated granular materials without gravity [33] or in low gravity [34,35] situations, particles form dense clusters away from the source and there is a continuous smooth variation of density from the dilute region to the dense region. In the present case there is a distinct phase separation occurring on the surface of the source and perpendicular to the direction of energy flux.

A stability analysis of the clustered state of [36] shows the existence of a localized clustered state [37]. This is also a coexistence of a dense and a dilute phase, perpendicular to the direction of the source, but it occurs at the elastic wall opposite the source. Here, the base state of the system itself has qualitatively different temperature and density profiles from the present ones, and the steady coexistence is obtained
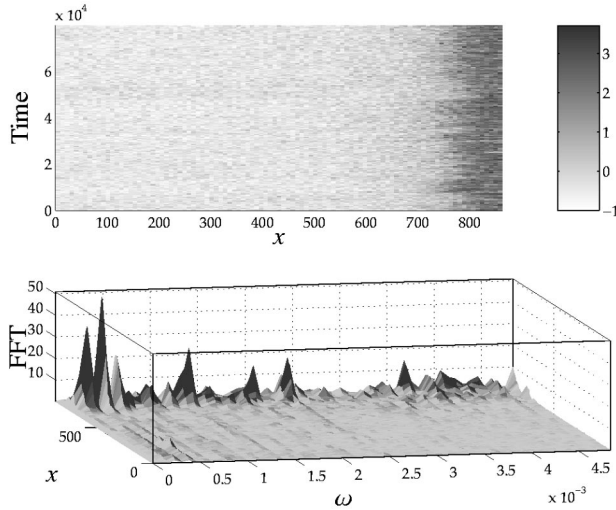
FIG. 14. Dynamics of the interface. A close inspection of the local scaled density fluctuations $\tilde{N}(x)$ in the top plot shows that the cluster interface is not static but varying with time. The second plot shows the fast Fourier transform (FFT) of the density fluctuation in the time domain at different horizontal positions. A peak is found at $x=770$ near the interface region. The characteristic radial frequency is around 4×10^{-4}, which corresponds to a time period of 1.6×10^4, roughly of the order of interface fluctuation in the top plot.

from the equations of hydrodynamics. In contrast, the coexistence in the present clustering instability possesses an oscillatory interface that cannot be explained by a simple steady state balance of fluxes [23,31], and therefore it is qualitatively different from [37]. Wavelike patterns have been observed for coexisting dense and dilute regions in vibrated layers, which oscillate subharmonically with the bottom wall vibrations [8,9]. But these states occur when the amplitude of vibrations is comparable to the layer thickness. In the present simulations the amplitude of vibrations is negligible compared to the height of the bed.

Phase separations have been observed in two-dimensional horizontal plane simulations [38] and experiments [14]. The constraints of the model and the experiments are such that the particles are restricted to move only in the two-dimensional plane. Here the coexistence is between an ordered (collapsed) phase and a liquidlike phase (which is referred to as "gaslike" in [14]). In contrast to this, in the present case the particles are in a fluidized state and the coexistence is between a gaslike region and a liquidlike region. For a monolayer of particles (at rest), the value of Γ in [14] is less than unity, whereas in the present case it is of $\mathcal{O}(100)$. Moreover, the clustering instability is observed only when the horizontal width is large enough. This instability also does not seem to occur with a constant temperature wall. These could be some of the reasons why the present instability was not observed in the earlier experiments and simulations of finite sized systems.

V. GENERAL RESULTS: PHASE DIAGRAM

We now examine the parameter regimes in the two controlling parameters where the phase separation and convec-
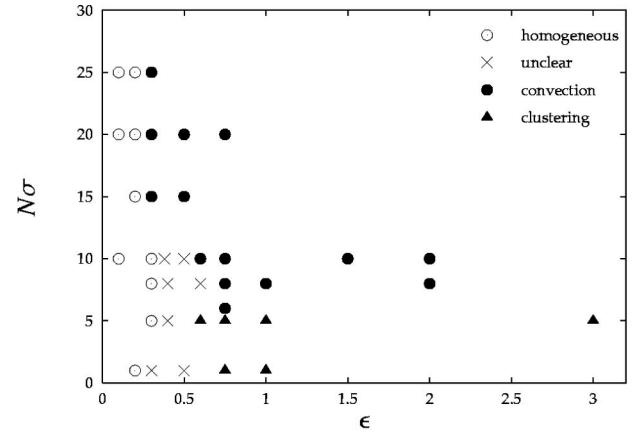
(a) points only
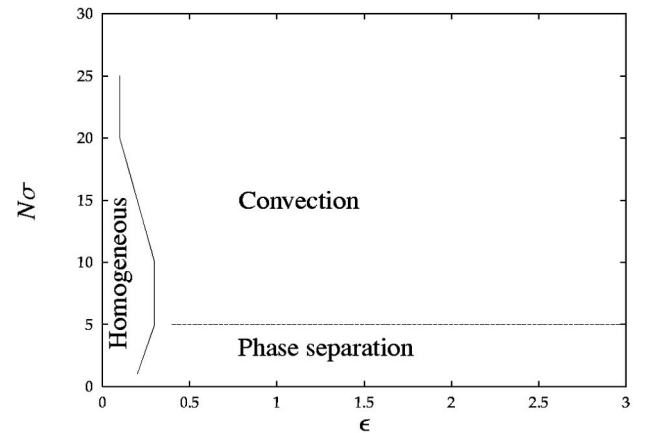
(b) approximate boundaries

FIG. 15. Phase diagram of an excited granular gas plotted in the $N\sigma$-ϵ plane. The system goes from a homogeneous to an inhomogeneous state as the dissipation (ϵ) is increased. For large values of $N\sigma$ the system forms convection rolls and for lower values a phase separation to two distinct phases occurs. The points marked ''unclear'' in (a) did not show any steady and clear density variation as opposed to the other points. (b) shows the approximate phase boundary obtained from (a). The other parameters are kept constant: $\nu^0=0.077$, $\epsilon_f=0.01$.

tive instabilities are encountered. The parameters are $N\sigma$, the product of the number of particles per unit width and the particle diameter, which is equal to the number of monolayers at rest, and ϵ, which is a measure of the rate of energy dissipation.

To obtain a phase diagram, we require an order parameter to quantify the state of the unstable system to distinguish it from the homogeneous state. We have tried out several order parameters [23], such as those reported in [6], but none of them could satisfactorily show a clear picture of the transition for different ranges of the parameters. Instead, in this section we present a phase diagram obtained by visual inspection of plots such as those in Figs. 1 and 2. Figure 15 shows the phase diagram in the $N\sigma$-ϵ plane. The instability sets in for very low values of dissipation parameter $\epsilon\approx0.3$. The transition from a phase separated state to convection is sharp and occurs around $N\sigma=5$.
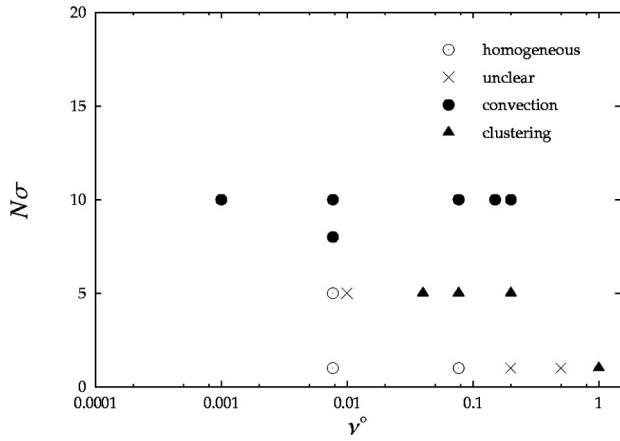
FIG. 16. The phase diagram in the $N\sigma$-ν^0 plane that can be realized experimentally. Here the amplitude of vibration is varied at a constant total number of particles so that the system goes from a homogeneous state to a phase separated/convection state. Note that the density is plotted on a logarithmic scale. The parameters that are kept constant are e, g, σ, W, and f_w (see text for details).

In a real experiment, the parameters that can be controlled are the the particle diameter σ and the number of monolayers at rest $N\sigma$. The acceleration due to gravity is fixed at $g = 9.8$ m s^{-2}, and the coefficient of restitution e of the particles is at most around 0.9. Commercial electromechanical vibrators operate at frequencies f_w in the range 20–1000 Hz, with amplitudes from 10^{-6} to 10^{-2} m. But the peak amplitudes of velocity U_0 that can be achieved are in the range 0.1–2 m/s. Particles are available in diameters of the order of 0.1–5 mm. The typical width of a vibrated bed can be of the order of 1 m. We have carried out simulations based on a set of data that can be realized experimentally. The following parameters are kept fixed:

$$e = 0.9, \quad \sigma = 1 \times 10^{-3} \text{ m}, \quad g = 9.8 \text{ m s}^{-2},$$

$$f_w = 60 \text{ Hz}, \quad W = 1 \text{ m},$$

and the following parameters are varied in the ranges indicated below:

$$N = 1000\text{--}10\,000 \text{ m}^{-1}, \quad a_w = 1 \times 10^{-4}\text{--}3 \times 10^{-2} \text{ m}, \tag{5}$$

which corresponds to the following values of the nondimensional numbers:

$$N\sigma = 1\text{--}10, \quad \epsilon = 0.2\text{--}2, \quad \nu^0 = 0.001\text{--}1,$$

$$\epsilon_l = 10^{-4}\text{--}1, \quad \epsilon_f = 0.01\text{--}2, \quad \epsilon_u = 0.03\text{--}1.$$

Figure 16 shows the phase diagram that can be realized experimentally. It is plotted between the number of layers at rest $N\sigma$ and the theoretical density at the bottom ν^0. Experimentally this would correspond to fixing the total number of particles N_p (i.e., along a constant $N\sigma$) and varying the amplitude of vibration from high to low (increasing ν^0). This takes the system from a homogeneous state to a convection
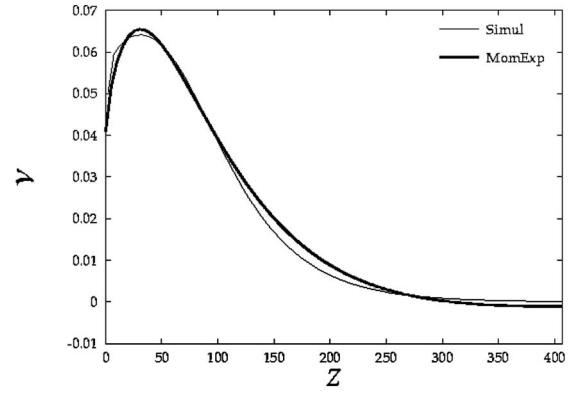
(a) Density profile
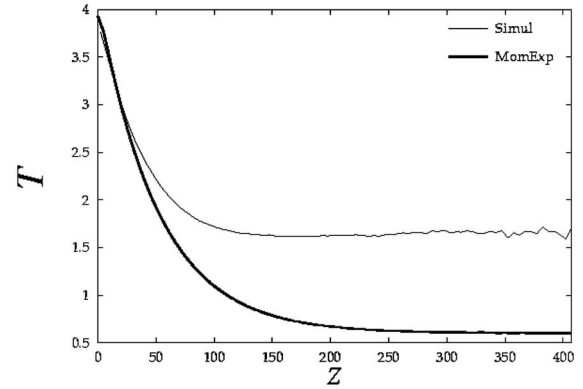
(b) Temperature profile
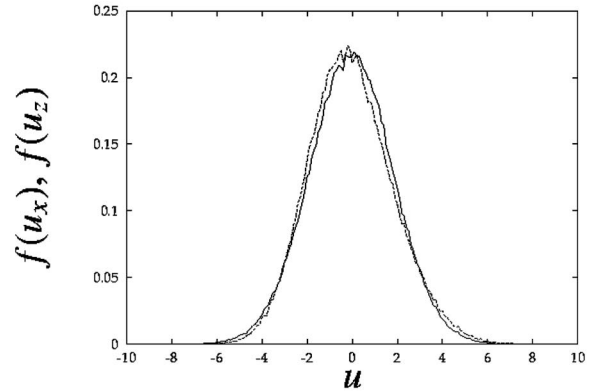
(c) Velocity distribution

FIG. 17. Comparison of simulation result (Simul) and moment expansion solution (MomExp) of [39]. (a),(b) Density and temperature profiles for a homogeneous case of a bed near the phase boundary of convection rolls. The parameters used for this simulation are $N\sigma = 10$, $\epsilon = 0.3$, and $\nu^0 = 0.077$. (c) shows the velocity distribution function near the bottom wall. The vertical velocity distribution $f(u_z)$ (dashed line) is only slightly away from the Gaussian horizontal velocity distribution $f(u_x)$ (solid line). The velocities are scaled by U_0.

or phase separated state as shown in the figure. The figure gives an indication of the regions where inhomogeneities occur.

It is useful to examine the state of the granular flow be-

fore the onset of instability, and determine whether this state can be adequately described by kinetic theory. The density and temperature profiles shown in Fig. 17 are calculated using the kinetic theory of vibrofluidized beds [23,39] for the parameter values just before the onset of convection. The increase in the density as well as the value of the temperature near the bottom are correctly captured. The velocity distribution function is also shown in Fig. 17. Both the horizontal and vertical velocity distributions are close to Gaussians. The homogeneous state of the bed just before the onset of a phase separation is also correctly captured by the theory [23].

VI. CONCLUSION

The instabilities in a dilute vibrated bed were analyzed in the limit where the amplitude of the bottom wall vibrations is small compared to the mean free path of the particles, and the frequency is large compared to the frequency of particle collisions with the wall. In this limit, three parameters $N\sigma$, ϵ, and ν^0, are required to specify the state of a system. Two instabilities were found—*convection rolls* and *phase separation.*

In most earlier studies, convection rolls occur at high densities and the frequency of motion is of the same magnitude as the frequency of the bottom wall vibration. We have shown that convection rolls can appear at low densities as well, and the frequency of the motion is small compared to that of the bottom wall vibration. Earlier studies [6] used a constant temperature condition at the bottom. The present simulations show that the onset of convection is sensitively dependent on the boundary condition at the bottom wall, and a constant temperature condition delays the onset of convec-

tion because it dampens horizontal fluctuations at the wall.

The clustering instability in the vibrated bed appears similar to that reported in [11], but a detailed analysis indicates that there are significant differences. A steady state flux balance analysis similar to that in [11] cannot be used to describe the phase separation in the present case. The coexistence of the two phases seems to be related to an oscillatory state of the interface and therefore the instability is qualitatively different from that in [11].

The instabilities were characterized using a ''phase'' diagram. At low values of $N\sigma$ a clustering instability occurs, and a convective instability at higher values. A recipe to observe these instabilities in a 2D experiment with a realistic values of the parameters was suggested. The variation of density and temperature in the homogeneous state just before the onset of convection/clustering is captured accurately by the kinetic theory of vibrated beds. This indicates that the stability of the system can be understood in terms of simple hydrodynamical equations.

The present simulations show that instabilities in vibrated granular media are more widespread than previously supposed, and they occur even in regimes where the dynamics is not correlated to that of the bottom wall vibrations, but where the bottom wall acts only as a source of energy in order to compensate for the energy dissipation due to inelastic collisions.

[1] M. Faraday, Philos. Trans. R. Soc. London **52**, 299 (1831).

[2] E. Clement and J. Rajchenbach, Europhys. Lett. **16**, 133 (1991).

[3] E. L. Grossman, Phys. Rev. E **56**, 3290 (1997).

[4] Y.-H. Taguchi, Phys. Rev. Lett. **69**, 1367 (1992).

[5] K. M. Aoki, T. Akiyama, Y. Maki, and T. Watanabe, Phys. Rev. E **54**, 874 (1996).

[6] R. Ramírez, D. Risso, and P. Cordero, Phys. Rev. Lett. **85**, 1230 (2000).

[7] S. Chandrasekhar, *Hydrodynamic and Hydromagnetic Stability* (Dover, New York, 1981).

[8] H. K. Pak and R. P. Behringer, Phys. Rev. Lett. **71**, 1832 (1993).

[9] S. Luding, E. Clément, J. Rajchenbach, and J. Duran, Europhys. Lett. **36**, 247 (1996).

[10] K. M. Aoki and T. Akiyama, Phys. Rev. Lett. **77**, 4166 (1996).

[11] J. Eggers, Phys. Rev. Lett. **83**, 5322 (1999).

[12] V. Kumaran, Phys. Rev. E **57**, 5660 (1998).

[13] Y. A. Beuvich and A. F. Ryzhkov, J. Eng. Phys. Therm. Phys. **626**, 1162 (1980).

[14] J. S. Olafsen and J. S. Urbach, Phys. Rev. Lett. **81**, 4369 (1998).

[15] S. B. Savage, J. Fluid Mech. **194**, 457 (1988).

[16] P. B. Umbanhowar, F. Melo, and H. L. Swinney, Nature (London) **382**, 793 (1996).

[17] K. Kumar, E. Falcon, K. M. S. Bajaj, and S. Fauve, Physica A **270**, 97 (1999).

[18] K. M. Aoki and T. Akiyama, Phys. Rev. E **58**, 4629 (1998).

[19] A. Puglisi *et al.*, Phys. Rev. Lett. **81**, 3848 (1998).

[20] J. S. Olafsen and J. S. Urbach, Phys. Rev. E **60**, R2468 (1999).

[21] W. Losert, D. G. W. Cooper, and J. P. Gollub, Phys. Rev. E **59**, 5855 (1999).

[22] F. Rouyer and N. Menon, Phys. Rev. Lett. **85**, 3676 (2000).

[23] P. Sunthar, Ph.D. thesis, Indian Institute of Science, Bangalore, India, 2001.

[24] C. S. Campbell, Annu. Rev. Fluid Mech. **22**, 57 (1990).

[25] M. Marin, D. Risso, and P. Cordero, J. Comput. Phys. **109**, 306 (1993).

[26] I. Goldhirsch and G. Zanetti, Phys. Rev. Lett. **70**, 1619 (1993).

[27] P. Sunthar and V. Kumaran, Phys. Rev. E **63**, 011508 (2001).

[28] C. E. Brennen, S. Ghosh, and C. R. Wassgren, Trans. ASME, J. Appl. Mech. **63**, 156 (1996).

[29] A. Goldstein, M. Shapiro, L. Moldavsky, and M. Fichman, J. Fluid Mech. **287**, 349 (1995).

[30] J. A. C. Gallas, H. J. Herrmann, and S. Sokolowski, Phys. Rev. Lett. **69**, 1371 (1992).

[31] P. Sunthar and V. Kumaran, e-print cond-mat/0103596.

[32] S. McNamara and W. R. Young, Phys. Rev. E **53**, 5089 (1996).

[33] Y. Du, H. Li, and L. P. Kadanoff, Phys. Rev. Lett. **74**, 1268 (1995).

[34] A. Kudrolli, M. Wolpert, and J. P. Gollub, Phys. Rev. Lett. **78**, 1383 (1997).

[35] E. Falcon *et al.*, Phys. Rev. Lett. **83**, 440 (1999).

[36] E. L. Grossman, T. Zhou, and E. Ben-Naim, Phys. Rev. E **55**, 4200 (1997).

[37] E. Livne, B. Meerson, and P. V. Sasorov, e-print cond-mat/0008301.

[38] X. Nie, E. Ben-Naim, and S. Y. Chen, Europhys. Lett. **51**, 679 (2000).

[39] V. Kumaran, J. Fluid Mech. **364**, 163 (1998).